Anti-thermal grain growth in $SrTiO_3$: Coupled reduction of the grain boundary energy and grain growth rate constant

Madeleine N. Kelly[1], Wolfgang Rheinheimer[2], Michael J. Hoffmann[2], and Gregory S. Rohrer[1]

[1]Department of Materials Science and Engineering, Carnegie Mellon University, Pittsburgh, Pennsylvania 15213, USA
[2]Institute of Applied Materials, KIT, Haid-und-Neu-Str. 7, 76131 Karlsruhe, Germany

Abstract

The dihedral angles at grain boundary thermal grooves in $SrTiO_3$ were measured and used to determine the relative grain boundary energy at several temperatures where the grain growth rate constant displays anti-thermal properties (it decreases with increasing temperature). The measurements indicate that at temperatures in the anti-thermal region (1390 °C – 1400 °C), the average grain boundary energy is less than at a lower temperature (1350 °C) where grain boundaries move more rapidly. Three-dimensional electron backscatter diffraction was used to measure the geometries of internal triple junctions in a sample where the slow and fast grain boundaries co-exist. Based on the dihedral angles at triple junctions, the ratio of the energies of slow boundaries to fast boundaries is 0.86. The results indicate that at temperatures between 1350 °C and 1425 °C, the higher and lower energy boundaries coexist. The coexistence of the two boundary types in this temperature range is likely because there is a range of grain boundary energies and the temperature at which a boundary transforms from the slow type to the fast type depends its grain boundary energy.

1. Introduction

In the vast majority of polycrystalline materials, grain boundaries migrate more rapidly at higher temperatures. According to the accepted theory of grain boundary migration, this is because as the temperature increases, atoms vibrate with an increased amplitude and the rate of diffusivity across the grain boundary increases [1]. The assumption of a temperature activated mechanism is supported by a vast amount of data indicating that boundaries migrate more rapidly at higher temperature both when the velocities of many boundaries are averaged [2, 3] and when individual boundary velocities are measured [4, 5]. However, some interesting contrary evidence has recently been reported [6]. For example, atomistic simulations have recently shown that certain grain boundaries have mobilities that are independent of temperature or move more slowly at elevated temperature [7]. Furthermore, recent experimental measurements of the grain growth rate constant in certain perovskite structured oxides have shown that over certain temperature ranges, the average grain growth rate constant decreases with increasing temperature [8]. The rate grain growth rate constant k is defined as [1]:

$$D^2 - D_{t=0}^2 = kt \tag{1}$$

where D is the average grain size and t is the time. For example, in $SrTiO_3$, the average grain growth rate constant decreases by a factor of 20 in the temperature range between 1350 °C and 1425 °C, as illustrated in Fig. 1 [8, 9]. We refer to this as anti-thermal behavior [6].

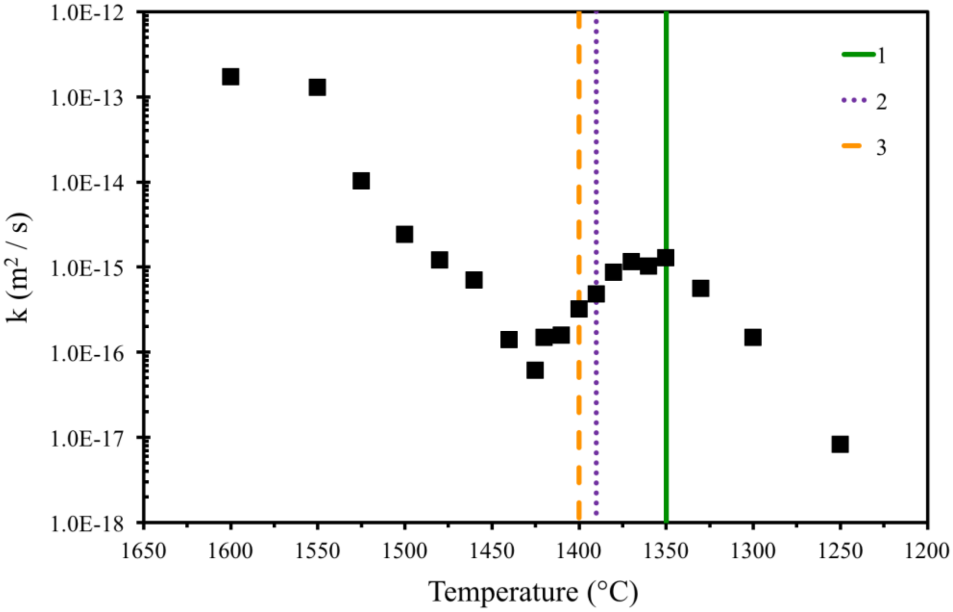

Figure 1. Grain growth rate constants (k) as a function of temperature for $SrTiO_3$ heated at various temperatures after pre-sintering at 1425 °C for one hour. 1, 2 and 3 refer to the three samples that are the focus of this study [8].

For the case of $SrTiO_3$, it is important to clarify that not all grain boundaries uniformly move more slowly in the anti-thermal temperature range. Up to 1350°C, all grain boundaries move at similar rates yielding uniform microstructures (Fig. 2a). Above 1350 °C, some grain boundaries move relatively more slowly than others as shown in Fig. 2b at 1400°C. At higher temperatures (e.g. 1425°C in Fig. 2c), a larger fraction of grain boundaries move slowly and fewer grain boundaries migrate quickly [8]. At 1425 °C, nearly all of the grain boundaries move relatively slowly. The effect of these changes is that the average grain growth rate constant decreases in this temperature range. At temperatures greater than 1425 °C, the grain growth rate constant is again thermally activated.

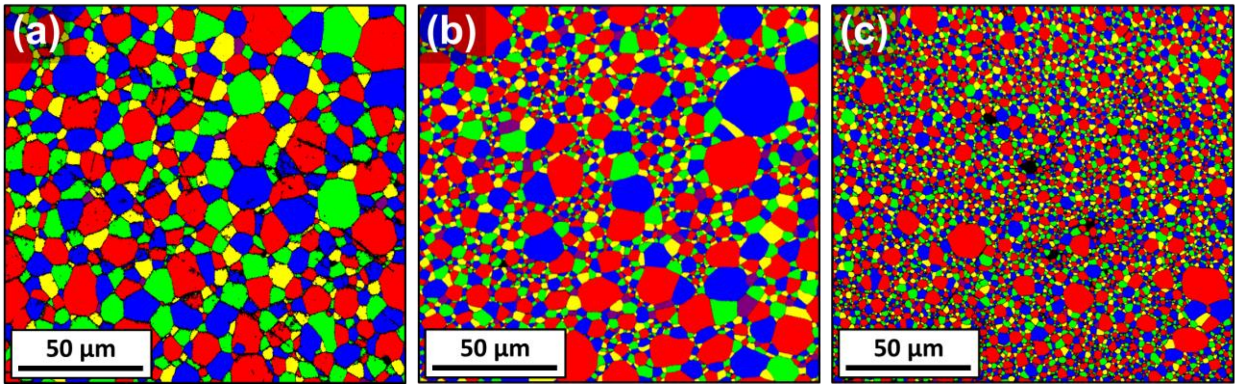

Figure 2. Images of the grain structure, measured by electron backscatter diffraction, illustrating the microstructures of $SrTiO_3$ after 10 h at (a) 1350°C, (b) 1400°C and (c) 1425°C [10].

The significant change in the rate of grain boundary migration and the co-existence of grain boundaries with significantly different migration rates has been observed in other ceramics, such as alumina doped with Ca, Si, or a variety of rare earth ions; in these situations, abnormal grain growth is observed [11]. The abrupt change in the migration rate of some boundaries has been explained by a grain boundary transition that alters the structure and composition of the grain boundary (also called the complexion transition), as well as its mobility [12]. Measurements of the relative grain boundary energy have shown that the complexion transition is associated with a decrease in the grain boundary energy [13, 14]. In other words, as temperature is increased, the grain boundary adopts a lower energy structure. A complexion transition seems to be a plausible explanation for the phenomenon in $SrTiO_3$ and this has been proposed in the past [9]. However, there are two significant differences between the phenomenon in $SrTiO_3$ and earlier studies of ceramics such as alumina [15], yttria [16], and spinel [17]. First, in these other cases, higher temperature complexions had higher mobilities than the lower temperature complexion; for $SrTiO_3$, the opposite is true. Of course, there is no intrinsic reason to believe that higher temperature complexions should always have higher mobilities. Second, TEM studies have yielded contradictory results with respect to structural differences between the fast and slow boundaries. Shih et al. [18] found that fast moving boundaries were often atomically flat with steps, while a later study found no significant structural difference between grain boundaries above and below the transition temperature [19]. Even though the samples were quenched, these room temperature microscopy experiments do not exclude the possibility that there are structural differences at temperatures where the grain boundaries are mobile.

The grain boundary free energy depends on temperature; for materials without strongly segregating impurities, the energy is expected to decrease continuously with temperature and for materials with segregating impurities, the energy is expected to increase continuously with temperature, at least until a point when there is no longer an excess of solute at the grain boundaries [20]. Complexion transitions should lead to more abrupt changes in the grain boundary energy [21, 22]. Furthermore, at temperatures where two grain boundary complexions coexist, the distinct populations have been shown to have distinct grain boundary energies [13]. If the change in grain boundary mobility that occurs in $SrTiO_3$ is the result of a complexion transition, then we expect the slower grain boundaries that are increasingly present at higher temperatures to have lower energies than the grain boundaries that move more rapidly at lower temperature.

The purpose of this paper is to determine if and how the grain boundary energy of $SrTiO_3$ changes in the anti-thermal temperature region where the grain growth rate constant decreases. We hypothesize the slower boundaries, which we refer to as S, and faster grain boundaries, which we refer to as F, have different complexions and different energies. To test this hypothesis, the relative grain boundary energies were determined from measurements of the grain boundary dihedral angles from two types of triple junctions. In one case, the relative energies were determined from the geometry of grain boundary thermal grooves of samples annealed at several temperatures. In the second case, three-dimensional reconstructions were used to measure the internal grain boundary dihedral angles in a sample where slow and fast grain boundaries co-exist. The measurements confirm that the grain boundary energy of the slow (S) boundaries is lower than that of the fast (F) grain boundaries, consistent with the idea that a grain boundary complexion transition changed the properties of the grain boundary.

2. Experimental

The preparation of the $SrTiO_3$ used in this study has been described in a previous publication [9]. Of relevance to the current paper, the samples were prepared to have a molar ratio (Sr/Ti) of 0.996. Also, ICP-OES was used to measure impurity concentrations (reported on a weight basis). The most concentrated impurities were Zr (600 ppm) and Y (35 ppm), which were probably introduced by the yttria stabilized zirconia milling media during the preparation of the powder. The sample also contained Ba (100 ppm) and Ca (250 ppm) and less than 10 ppm of Al, Cr, Mg, Fe, Nb, Ni and Mn. These impurities are expected to be below the solubility limit. Before any other heat treatments, the green bodies were pre-sintered by heating at 20 °C/min to 1425 °C and holding for one hour in oxygen. After the pre-sintering, but before cooling, the furnace temperature was changed to a temperature between 1350 °C to 1550 °C at 20 °C/min. The samples were then annealed in oxygen for an additional 10 h before quenching in oxygen.

After heat treatment, the samples were cut into ~ 1 mm thick slices and polished on one side. The cut and polished samples were then annealed to create grain boundary thermal grooves. The annealing durations were selected to achieve groove widths greater than 0.5 μm. The samples were gas quenched following grooving. The preparation conditions are specified in Table 1. Atomic force microscopy (AFM) was used to measure the shapes of the grain boundary thermal grooves and determine the relative grain boundary energy for samples annealed at temperatures ranging from 1350 °C to 1550 °C. The procedure for measuring the grooves and determining the relative grain boundary energies has been described in detail previously [21, 23]. Briefly, Gwyddion post-processing software [24] was used to extract three height profiles along lines perpendicular to a grain boundary, as illustrated in Fig. 3. The depth (d) and width (W) of each profile was extracted using a computer program and the relative grain boundary energy (the ratio of grain boundary to surface energy) was computed using Equation 2. [25]

$$\frac{\gamma_{gb}}{\gamma_s} = 2sin\left(tan^{-1}\left(m\left(\frac{d}{2W}\right)\right)\right) \qquad (2)$$

In Equation 2, γ_{gb} is the grain boundary energy, γ_s is the surface energy, and *m* is a function that relates *d* and *W* to the groove angle, β, defined in Fig. 3. Throughout this paper, we will refer to the ratio, γ_{gb}/γ_s, as the relative grain boundary energy. Details about these measurements and the function *m* are described in earlier publications [21, 23]. When the relative grain boundary energy is measured from a grain boundary thermal groove, the value obtained is sensitive to the particular type of grain boundary, the surfaces bounding the groove, and its inclination. Here, we measure a distribution of values from approximately 200 grain boundaries and take the mean of the distribution to represent the grain boundary energy at a particular annealing temperature. Previous work has shown that the uncertainty in the mean value depends on the number of measurements in the distribution and that it is smaller than other uncertainties after about 100 measurements of randomly selected boundaries [21, 23]. The number of boundaries measured for each $SrTiO_3$ sample is listed in Table 1.

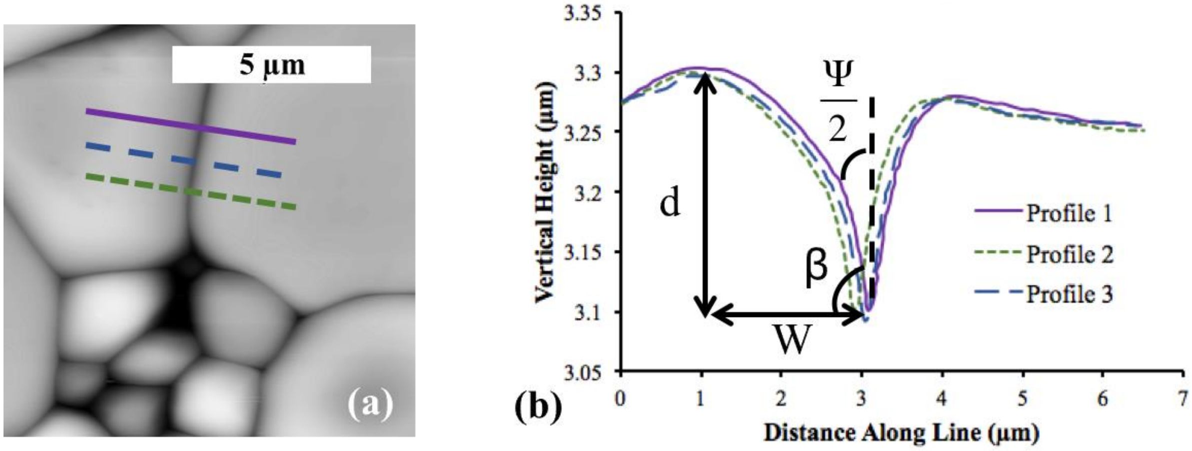

Figure 3. Example of a grain boundary groove measurement in $SrTiO_3$. Three profiles are extracted from the topographic AFM image in (a). The depth (d) and width (W) of the groove are measured from the topographic data. The results from the three profiles are averaged to determine the result for this grain boundary.

Table 1. Sample Preparation Conditions and Number of Grooves Measured

Sample	Sintering conditions	Annealing conditions	Grooving conditions	Grooves measured
1	1425 °C/ 1 h	1350 °C/ 10 h	1350 °C/ 40 min	208
2	1425 °C/ 1 h	1390 °C/ 10 h	1390 °C/ 20 min	200
3	1425 °C/ 1 h	1400 °C/ 10 h	1400 °C/ 20 min	192

A persistent problem with measuring grain boundary groove profiles by AFM is that the shape of the tip can change during the measurement and influence the apparent depth, leading to inconsistent results. To obtain reproducible and accurate results, a new procedure was introduced in this work. We measure grain boundary thermal grooves on a standard sample before and after data collection. If the measurements after data collection do not match the values before (within typical uncertainty), the data is discarded. Measurements of the relative grain boundary energy were deemed acceptable if measurements of the standard before and after the acquisition of data from $SrTiO_3$ differed by less than 0.1 arbitrary units (the units of the relative grain boundary energy). If the relative grain boundary energies on the standard sample differed from expectations by more than 0.1, the AFM tip was replaced and, when necessary, the instrument was re-calibrated before collecting additional data.

Some of the samples we examined proved unsuitable for the thermal groove measurements. First, samples heated at temperatures greater than 1425 °C showed the presence of an intergranular phase, identified as rutile structured titania. This is hardly surprising considering that the samples were formulated to be rich in titania. For example, many of the grain boundaries in the sample heated at 1550 °C were wet by an intergranular phase; therefore, the surface groove geometry is determined by the two-phase interface rather than a $SrTiO_3$ grain boundary. Also, the sample heated at 1425 °C has a very small grain size, with grain diameters in the 1 to 2 μm range. For grains of this size, the grooves from the grain boundaries overlap, and the grain surface has a single rounded shape, rather than the distinct shape of independent grain boundary grooves. In such cases, the width of the apparent groove is determined by the grain size and the grain boundary energy.

Therefore, measurements from such surfaces cannot be interpreted using Equation 2. Attempts to limit the groove size by annealing at lower temperatures led to highly faceted grain surfaces, which also obscured the groove profile. As a result of these limitations, we focus on results from the samples heated at 1350 °C, 1390 °C, and 1400 °C. As illustrated in Fig. 1, this provides a sample of grain boundaries just before the anti-thermal region (1350 °C) and two samples within the anti-thermal region. In these samples, grooves were only measured from grains where independent grooves were observed in the AFM images and this occurred only for grains with diameters greater than or equal to approximately 3 μm.

The dihedral angles at internal grain boundary triple junctions in the sample prepared at 1390 °C were computed from three-dimensional electron backscatter diffraction (EBSD) data. The procedures for identifying the geometry of the triple lines and the adjoining grain boundaries have been described previously [26, 27]. With knowledge of the normal vector to each grain boundary plane, three dihedral angles are easily computed. The input for the analysis is a set of parallel EBSD maps. The sample was prepared for the serial sectioning experiment by fracturing a thin (~ 30 μm) sample with a razor blade and mounting the sharpest fragment onto the 36° side of a 36° / 54° pre-tilted holder with silver paint. FEI's Helios™ Xe plasma focused ion beam (PFIB) dual-beam scanning electron microscope was used for the serial sectioning experiment. The experimental set-up and procedures have already been described in detail [28]. The serial sectioning was accomplished by milling away thin layers (100 nm) with the PFIB. The FEI AutoSlice and View (EBS3 G3) software was used to control the milling and Oxford's AztecHKL system was used to obtain orientation mapping for each slice. The samples were ion milled at 30 kV and 15 nA using a 5° rocking mill. EBSD orientation maps were collected with the camera was set to 4 x 4 pixel binning, an integration time of 2.3 ms, a camera gain of 15, and two frames were averaged for each point. For indexing, we used band center detection, refined accuracy, auto and static background collection, a Hough resolution of 80, and orientations were determined from 12 bands.

The first step of processing the data was a clean-up using the TSL OIM software. The clean-up procedure started with of a grain dilation operation with a minimum grain size of 5 pixels and minimum misorientation angle of 5°. This was followed by assigning a single average orientation per grain and a grain confidence index standardization. The grain boundaries were then approximated as line segments in each plane, such that the approximate boundary position differed from the true position by no more than two pixels. An example orientation map with the approximated grain boundary line segments is illustrated in Fig. 4. At the end of this procedure, the coordinates of each line segment were exported with the orientations and unique numerical identifiers (IDs) of the grains on either side of the segment. The same software also used to produce a list of grain sizes linked to the grain ID.

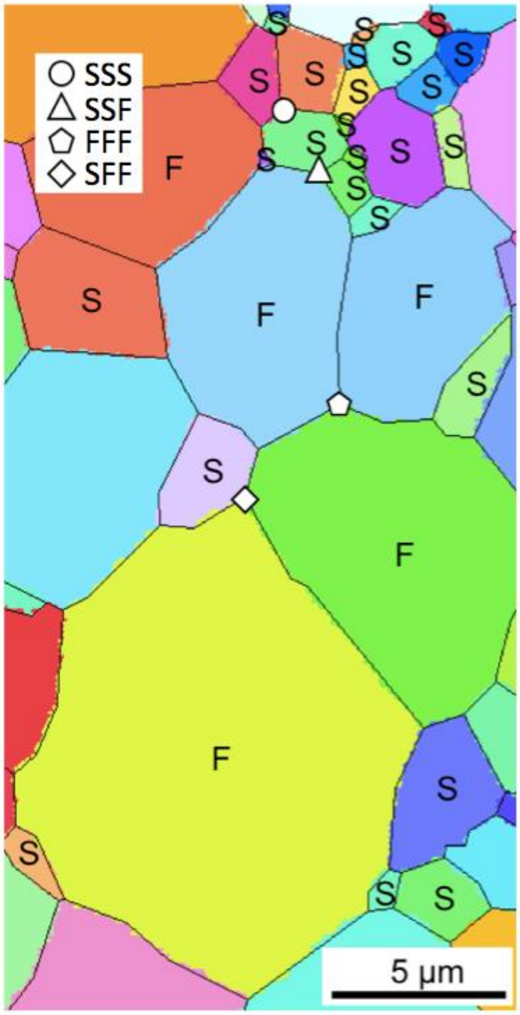

Figure 4. Grain orientation map of a single layer of the SrTiO$_3$ sample annealed at 1390 °C. Regions of the same orientation have the same color and the line segments approximating the grain boundaries are represented as black lines. Grains not touching an edge were labeled 'S' if they have an equivalent circular diameter < 5 μm and 'F' if they are larger. Four exemplary triple lines of different types are marked (see detailed explanation in text).

Based on the grain size, each grain was designated at small or large. Throughout this paper, small grains will be designated as type 'S' and large grains as type 'F'. In Fig. 5, the grain sizes extracted from three characteristic, non-contiguous, two-dimensional layers within the analyzed volume are ranked. For the smallest grains sizes, there is a linear increase in size with rank. There is an abrupt change in slope at a grain diameter of about 5 μm, so this was selected as the dividing line between the large and the small grains. The grains in Fig. 4 are labeled according to this criterion. This makes it possible to define three different types of grain boundaries (GB): those between two small grains (GB_{SS}), those between two large grains (GB_{FF}), and those between a small and large grain (GB_{SF}). These boundaries can create four types of triple junctions (TJs): those where three SS GBs meet (TJ_{SSS}), those where three FF GBs meet (TJ_{FFF}), those where a SS GB meets two SF GB (TJ_{SSF}), and those where a FF GB meets two SF GB (TJ_{SFF}). An example of each type of GB and TJ is illustrated in Fig. 6. The dihedral angles were classified according to their grain boundary type.

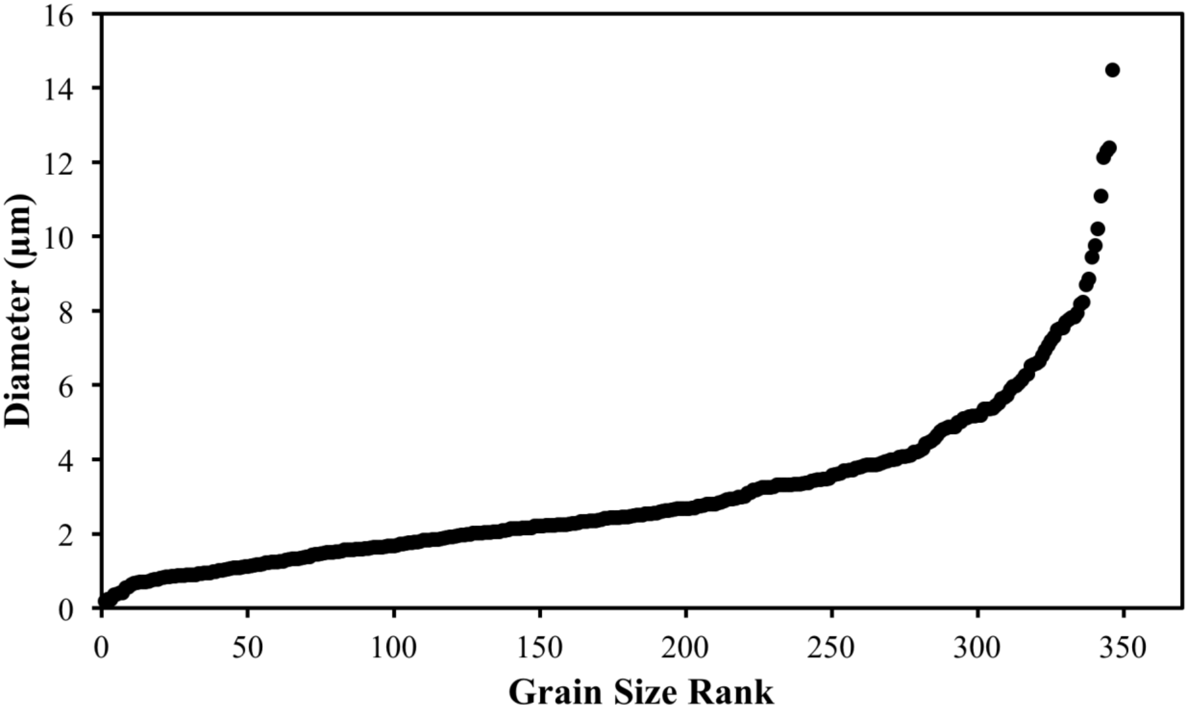

Figure 5. Grain sizes versus grain size rank for all of the grains within three parallel layers of the three-dimensional data. Grains touching the edge of the micrograph were ignored. There is an abrupt change in the slope at a diameter of about 5 μm, which we select as a condition to separate small and large grains.

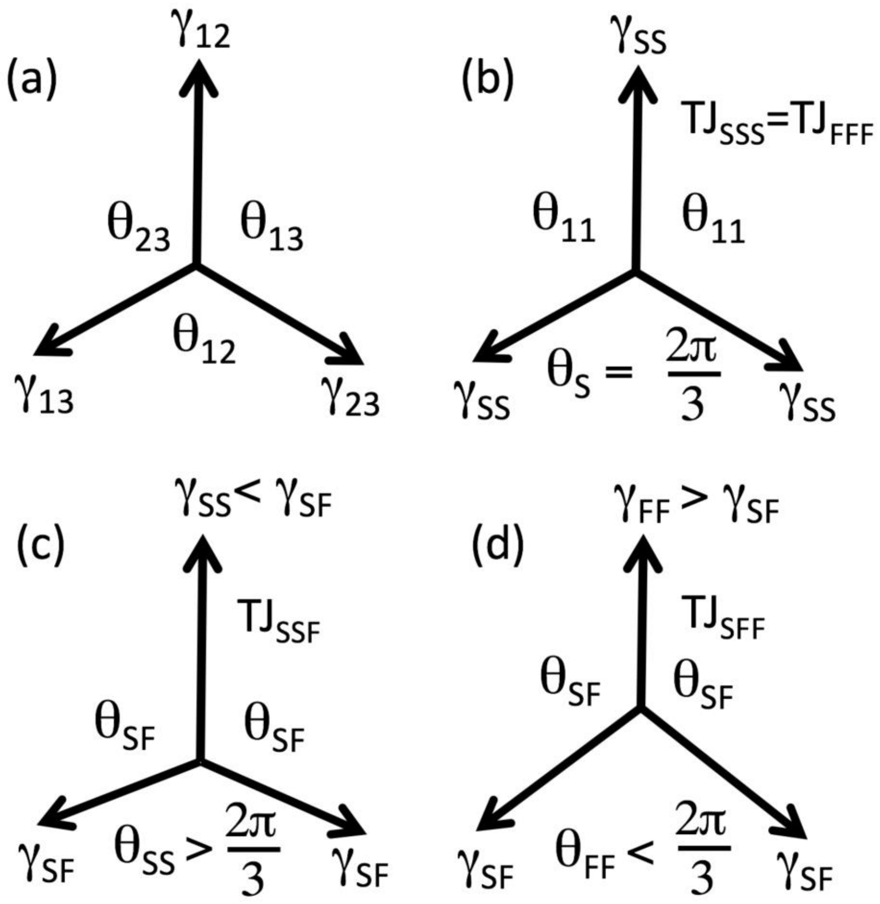

Figure 6. Triple junction schematics. (a) Schematic defining energies and dihedral angles from Equation 3. (b) The ideal case for when three GB_{SS} meet. The ideal case for three GB_{FF} is analogous. (c) The ideal case for when a GB_{SS} (with lower relative energy) meets two GB_{SF} boundaries. (d) The ideal case for when a GB_{FF}(with higher relative energy) meets two GB_{SF}.

The Young equation [29] gives:

$$\frac{\gamma_{12}}{\sin\theta_{12}} = \frac{\gamma_{23}}{\sin\theta_{23}} = \frac{\gamma_{13}}{\sin\theta_{13}} \qquad (3)$$

The parameters in equation 3 are defined in Fig. 6(a). If the hypothesis that a complexion transition occurs is valid, then we can state the following expectations about the dihedral angles. First, if three grain boundaries of the same type meet (at TJ_{SSS} or TJ_{FFF}), then the average dihedral angle should be 120° (see Fig. 6(b)). Second, if grain boundaries of type SS have a systematically lower energy than the others, their average dihedral angle at junction types SSF should be greater than 120° (see Fig.6(c)). Third, if grain boundaries of type FF have a systematically higher energy than the others, their average dihedral angle at junction types SFF should be less than 120° (see Fig. 6(d)).

3. Results

The topographic AFM images in Fig. 7 illustrate typical areas of the $SrTiO_3$ surfaces annealed at 1350 °C, 1390 °C, and 1400 °C. Numerous similar images of each sample were accumulated so that the profiles of approximately 200 grooves could be recorded. A higher resolution example of one groove is shown in Fig. 3. The mounds on either side of the groove are consistent with the shape expected when the groove is formed by surface diffusion [25]. The parameters needed as input for Equation 2, W and d, are determined by averaging values from three parallel profiles.

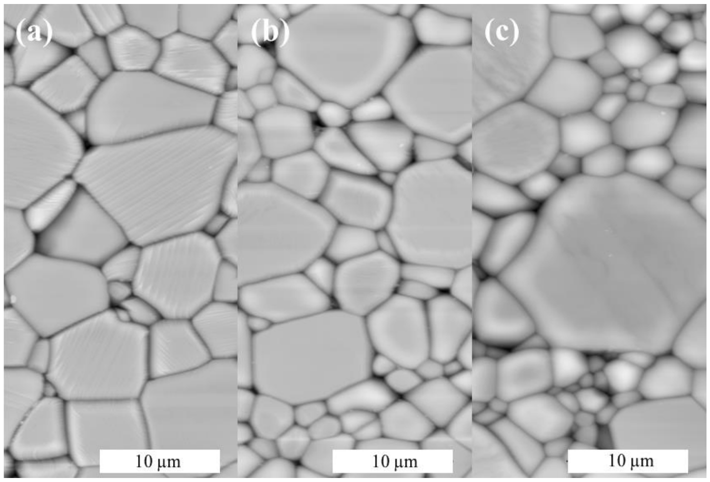

Figure 7. Representative topographic AFM images of the samples annealed at (a) 1350 °C, (b) 1390 °C, and (c) 1400 °C.

The distributions of the relative energies, determined from Equation 2, are shown in Fig. 8. From these distributions, it is clear that the average of the relative grain boundary energy at 1350 °C is the highest, with a mean value of 0.87. The uncertainty of this value, determined from the variations found in random subsets of the data [21], is ± 0.01. The averages for the relative grain boundary energies for the samples annealed at 1390 °C and 1400 °C are 0.73 and 0.80, respectively, with a similar uncertainty. Therefore, according to the thermal groove data, the average grain boundary energy in the anti-thermal range is lower than at 1350 °C.

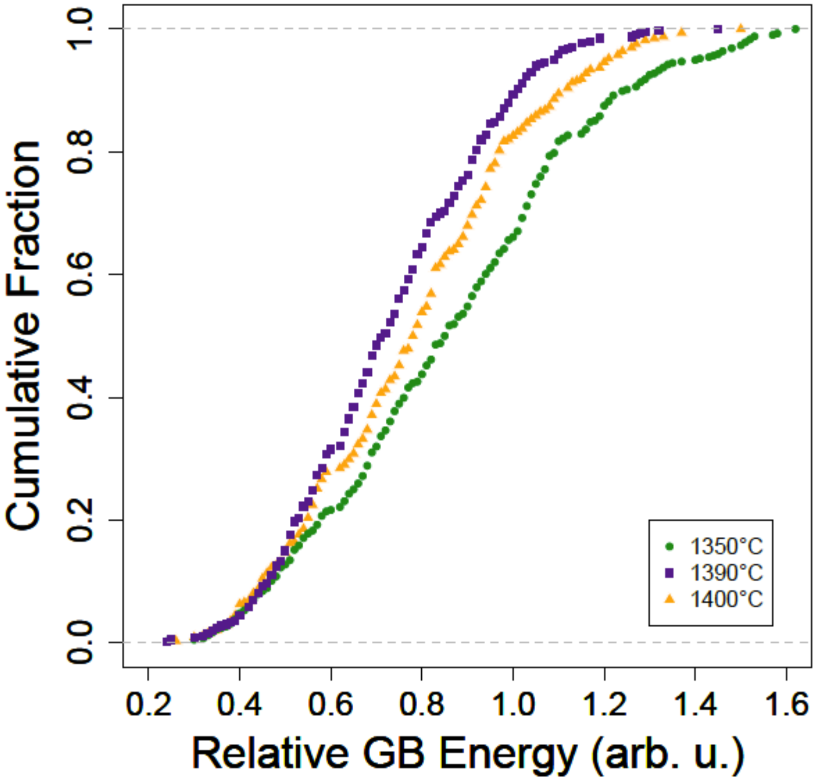

Figure 8. Relative grain boundary energy distributions for the samples heated at 1350 °C, 1390 °C, and 1400 °C. Each point corresponds to a measured grain boundary groove and the points are ordered by relative energy.

The difference from result at 1390 °C and 1400 °C is unexpected and may be the result a bias in the way the grain boundaries are sampled, with more of the fast boundaries being sampled at 1400 °C than at 1390 °C. As is illustrated by the energy distributions in Fig. 8, grain boundaries with a wide range of energies contribute to the average. It is important to remember that no attempt was made to separate data from boundaries around large and small grains; data was collected from any grain with clearly formed grooves and this was from grains larger than about 3 μm. This will naturally include some slow boundaries (from grains smaller than 5 μm) and some fast boundaries (from grains larger than 5 μm). As is evident in Fig. 7, the 1400 °C microstructure has more small grains below the size threshold for reliable groove measurements. Therefore the distribution likely samples a larger fraction of large grains. Assuming the boundaries around large grains have energies similar to the sample at 1350 °C, this bias can lead to a higher estimate for the mean energy.

A three dimensional reconstruction of the microstructure of the sample heated at 1390 °C is shown in Fig. 9. The volume illustrated consists of 28 parallel EBSD maps, each with a field of view of 29 μm x 44 μm separated by 100 nm. A smaller volume (not shown) that consists of 13 parallel layers with the same dimensions and spacing was also included in the analysis. The smaller volume was parallel to, but not perfectly connected with, the larger volume illustrated in Fig. 9. When the triple junctions were analyzed, there were 1,743 examples of $\mathrm{TJ}_{\mathrm{SSF}}$, where one $\mathrm{GB}_{\mathrm{SS}}$ met two $\mathrm{GB}_{\mathrm{SF}}$ and 529 examples of $\mathrm{TJ}_{\mathrm{SFF}}$, where one $\mathrm{GB}_{\mathrm{FF}}$ met two $\mathrm{GB}_{\mathrm{SF}}$. The distributions of dihedral angles for the $\mathrm{GB}_{\mathrm{SS}}$ and $\mathrm{GB}_{\mathrm{FF}}$ at these triple junctions are shown in Fig. 10. The most common type of triple junction was where three $\mathrm{GB}_{\mathrm{SS}}$ met ($\mathrm{TJ}_{\mathrm{SSS}}$) or three $\mathrm{GB}_{\mathrm{FF}}$ met ($\mathrm{TJ}_{\mathrm{FFF}}$). There were more than 8000 of these and their distribution is also shown in Fig. 10. Note that the dihedral angles for this last type of junction have mean values of 120°, as expected. When the dihedral angle distributions from the TJ_{SSS} and TJ_{FFF} are considered separately, the mean values are also 120°. The mean value for the dihedral angle of GB_{SS} (GB_{FF}) at TJ_{SSF} (TJ_{SFF}) is 125° (115°). This suggests that the boundaries between the small grains have energies that are, on average, lower than the rest of the population and boundaries between larger grains have energies that are, on average, higher than the rest of the population. We note that the distributions have varying degrees of skew, so that the mean and the median values of the distributions are not the same. The median values of the angles for TJ_{SFF}, TJ_{SSS} (TJ_{FFF}), and TJ_{SSF} are 116°, 123°, and 130°, respectively. Note that while the values are different than the mean, the ordering of the energies that would be derived from these angles is the same.

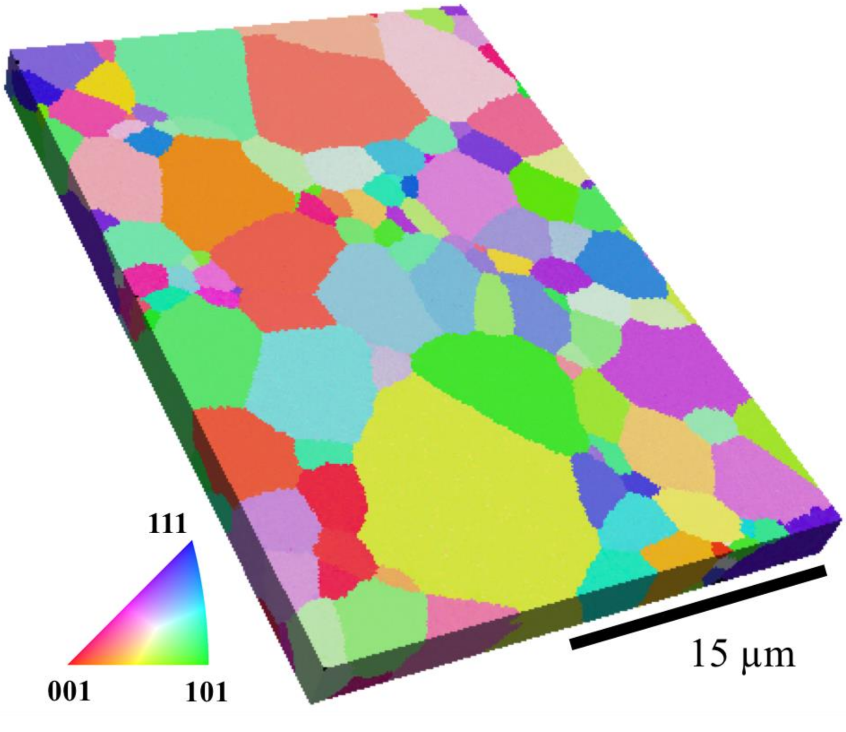

Figure 9. Three-dimensional reconstruction of the microstructure of the $SrTiO_3$ sample annealed at 1390 °C. The grains are colored by orientation. The triple junction dihedral angles were calculated from these data.

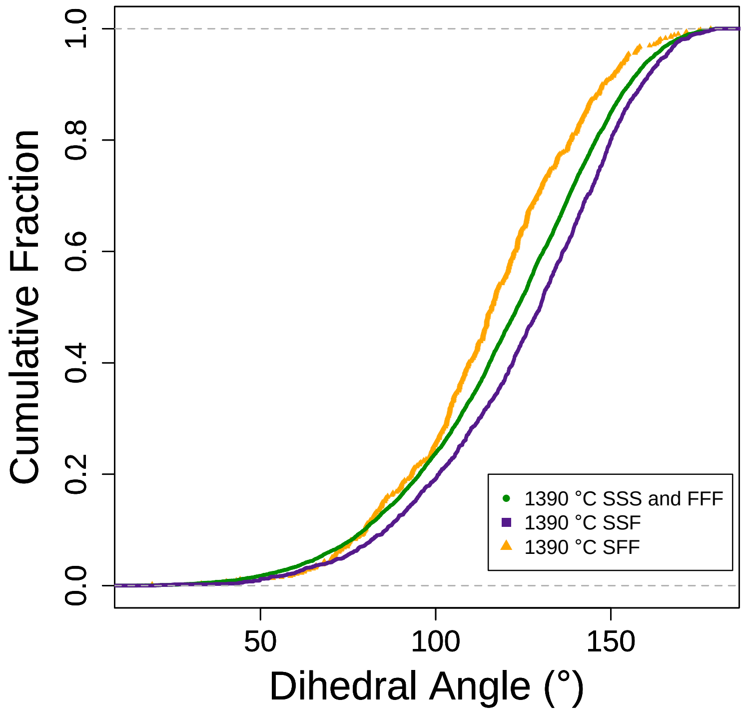

Figure 10. Distribution of grain boundary dihedral angles for type SFF triple junctions, type SSF triple junctions, and the combined type SSS and FFF junctions.

4. Discussion

The results from the analysis of grain boundary thermal grooves and from internal triple junctions yield consistent results. Namely, the grain boundaries around larger grains, that move more rapidly, have systematically higher energies than the grain boundaries around the smaller grains that move more slowly. This is consistent with the hypothesis that above 1350 °C, there is a complexion transition that reduces the grain boundary energy. From the thermal groove measurements, the energy at 1390 °C (1400

°C) is reduced by 16 % (8 %) compared to the energy at 1350 °C. These magnitudes are consistent with energy reductions reported for other complexion transitions [15, 21, 30].

As mentioned earlier, these energies are determined from averages. We can also estimate energy changes from dihedral angles observed at internal junctions. Rearranging the terms in Equation 3, we can estimate the energy ratios for type SS and FF grain boundaries to type SF grain boundaries in the following way:

$$\frac{\gamma_{SS}}{\gamma_{SF}} = \frac{\sin\theta_{SS}}{\sin(\frac{1}{2}(2\pi - \theta_{SS}))} \tag{4}$$

$$\frac{\gamma_{FF}}{\gamma_{SF}} = \frac{\sin\theta_{FF}}{\sin(\frac{1}{2}(2\pi - \theta_{FF}))} \tag{5}$$

Inserting the measured average dihedral angles, we find that $\gamma_{SS}/\gamma_{SF} = 0.92$ and $\gamma_{FF}/\gamma_{SF} = 1.07$. In other words, the boundaries between the smaller grains, that we assume are in the S state, are lower in energy than the boundaries between smaller and larger grains. Also, the boundaries between the larger grains, characteristic of the lower temperature F state, are greater in energy. The ratio of the energies of the high temperature to low temperature complexion is $\gamma_{SS}/\gamma_{FF} = 0.86$. If we consider the ratio of the relative energies at 1390 °C and 1400 °C (majority type SS grain boundaries) to the relative energy at 1350 °C (majority type FF grain boundaries) determined from the thermal grooves, it is 0.92 and 0.84. Note that the estimate from internal triple junctions (0.86) falls between the two estimates from the grain boundary thermal grooves. If we average the relative energy at 1390 °C and 1400

°C and compare it to the average energy at 1350°C, γ_{SS}/γ_{FF} = 0.88, consistent with the value derived from the internal junctions.

The temperature is known to affect grain boundary energies and because the groove measurements were made on samples annealed at different temperature, one would expect different energies. In materials without strongly segregating impurities, the grain boundary energy decreases with temperature because of the increasing importance of the entropy to the free energy. The main impurities in the $SrTiO_3$ studied here are Y and Zr, which are known to dissolve readily in $SrTiO_3$, and are therefore not expected to segregate strongly. The decrease in grain boundary free energy with increasing temperature has been observed experimentally in Ni and Cu [20] and also in atomistic simulations [31, 32]. However, the change from entropy alone is thought to be smaller than what was observed here between 1350 °C and 1400 °C [20]. For example, in Ni, the grain boundary energy decreases by about 4 % per 100 °C from 0 K to the melting point [31]. This is much smaller than the observed decrease over 50 °C in the present study. It should also be noted that the groove measurements are affected by changes in the surface energy with temperature. However, the temperature sensitivity of the surface energy is less than the grain boundary energy [33]. Also, because the groove measurements are consistent with the internal triple junction measurements, which are not influenced by the surface, we conclude that changes in the surface energy do not play an important role.

The coexistence of two different types of grain boundaries with different average energies can be explained if we assume that there is a temperature range over which the grain boundaries transform from one type to the other. This may be because of there is a barrier to the nucleation of the complexion [34]; it would also be a natural consequence of the grain boundary energy anisotropy [35]. It has been suggested that higher energy grain boundaries should transform to lower energy complexions at lower temperatures than low energy grain boundaries [35] and there is experimental support for this suggestion [15]. In this case, the majority of the boundaries transform in the temperature region between 1350 °C and 1425 °C. This is illustrated schematically in Fig. 11, where it is assumed that grain boundary free energies of the two complexions decrease with temperature and have different slopes. The mean grain boundary free energies are shown as lines. There are shaded bands around each of these lines to represent the distribution of grain boundary energies for different types of grain boundaries. With reference to the schematic in Fig. 11, the fast GB complexion is stable for nearly all boundaries types below 1350 °C. Similarly, the slow GB complexion is stable for nearly all boundaries types above 1425 °C. Between these two temperatures, there is a co-existence of the two types of grain boundaries. The results suggest that the when the sample is heated in the anti-thermal range, differing amounts of the fast boundaries form among the slow boundaries that are created during the pre sintering treatment at 1425 °C. The fraction of each grain boundary type that appears in the population depends both on the grain boundary energy anisotropy and kinetics for transformation to the equilibrium complexion. Thus, when the dihedral angles are measured, the boundaries between the larger grains (fast) are higher in energy than those between the smaller grains (slow). It is the coexistence of the two grain boundary types that makes it possible to measure distinct dihedral angle distributions at 1390 °C.

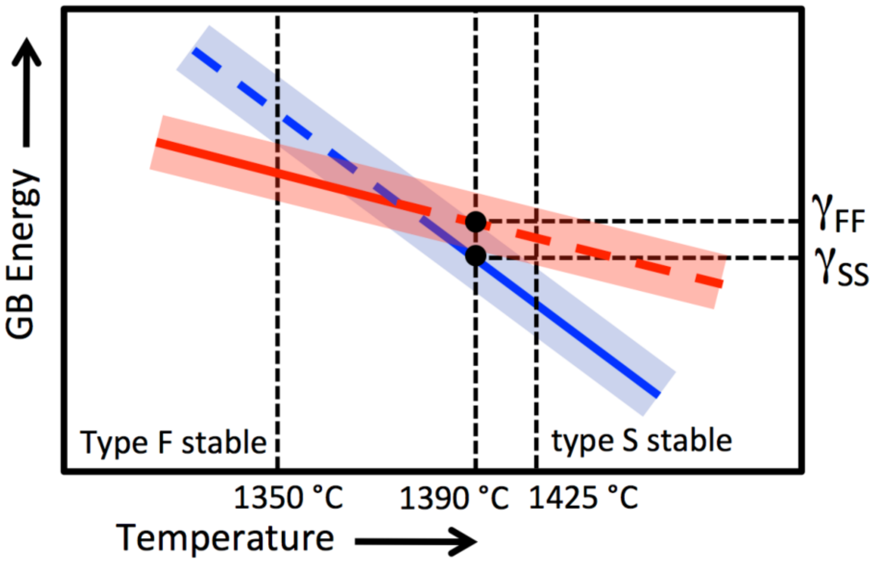

Figure 11. Schematic diagram to explain the change in grain boundary energy within the anti-thermal region. The lines indicate the mean energies and the shaded bands indicate the range of energies resulting from anisotropic grain boundary energies. The lines are dashed when the complexion (based on its mean energy) is metastable and solid when it is stable.

It is important to emphasize that the relative energies discussed above are averages and, in reality, it is known that the surface and grain boundary energy of $SrTiO_3$ is anisotropic [36, 37]. Therefore, if the grain boundary texture changes, this will also influence the average grain boundary energy. Rheinheimer et al. [38] compared the grain boundary plane distributions in $SrTiO_3$ at 1350 °C and 1425 °C and found that in the sample dominated by slow boundaries, there was a higher relative area of grain boundaries terminated by (100) planes, which are thought to have relatively lower energy [37]. This consistent with the present measurements showing that slow boundaries have lower energy. Note that it is not practical to decouple the change in the grain boundary plane distribution from the grain boundary energy. A range of past measurements have shown that the relative grain boundary area and energy distributions are coupled [26, 27, 39, 40] and this is thought to be caused by a bias for eliminating high energy grain boundaries during grain growth [41]. As noted above, this anisotropy is likely to be the cause of the co-existence of the slow and fast grain boundaries in the anti-thermal region. The lowest energy fast (slow) boundaries will require the greatest super heating (super cooling) to induce the transformation to the slow (fast) grain boundary complexion.

The observation that as the lower energy slow grain boundaries increase in the population, the relative area of grain boundaries with the (100) orientation also increases, is contradictory to HRTEM observations reported by Shih et al. [18]; in this earlier work it was reported that atomically flat boundaries with one grain face oriented in the (100) direction were associated with the fast grain boundaries (here, type F). The origin of this difference is not clear. However, it is worth noting the atomically flat (100) boundaries always made up a minority fraction of all grain boundaries examined by Shih et al. [18]. For example, they made up 45 % of the boundaries observed on abnormally large grains, 28 % of boundaries between smaller grains, and 34 % of all (71) grain boundaries imaged.

An obvious question is, how does the decrease in grain boundary energy influence the grain growth rate constant? The grain boundary energy makes a linear contribution to the grain boundary velocity. So, a decrease in energy will reduce the rate of grain growth. However, and average decrease in energy of 14 % is unlikely to lead to the significant decrease in the grain growth rate constant that is observed [9]. Furthermore, there are many documented cases where a decrease in grain boundary energy is associated with a complexion transition leads to an increased rate of grain growth [13, 16]. Therefore, it seems more likely that there is also a change in grain boundary structure or chemistry that changes the rate of migration. While the motion of steps across flat interfaces have been noted as a mechanism of grain boundary motion in both HRTEM studies [18, 19], clear differences above and below the transition temperature are not yet apparent.

4. Conclusion

A complexion transition that lowers the energies of grain boundaries in $SrTiO_3$ occurs in the temperature range between 1350 °C and 1425 °C. Two grain boundary complexions coexist in this temperature range, where the microstructure is bimodal. The grain boundaries around the larger grains have a greater energy and migrate faster than the boundaries around the small grains that have a lower energy. The ratio of the grain boundary energies for the slow and fast boundaries is 0.86. We conclude that the anti-thermal behavior of the grain growth rate constant is the result of a grain boundary complexion transition that creates lower energy, slower moving grain boundaries at temperatures greater than 1350 °C.

Acknowledgement

G.S.R. acknowledges equipment support from the National Science Foundation under MRI grant DMR 1428480 and research support from National Science Foundation (DMREF-1628994). M.N.K. acknowledges support from the ONR-MURI program (grant no. N00014-11-0678). W.R. acknowledges funding from the German Science Foundation (DFG grant no. HO 1165/20-1) and the German-Israel Fund (GIF, grant no. I-1276-401.10/2014). The authors acknowledge the use of the Materials Characterization Facility at Carnegie Mellon University supported by grant MCF-677785.

Figure Captions

Figure 1. Grain growth rate constants (k) as a function of temperature for $SrTiO_3$ heated at various temperatures after pre-sintering at 1425 °C for one hour. 1, 2 and 3 refer to the three samples that are the focus of this study [8].

Figure 2. Images of the grain structure, measured by electron backscatter diffraction, illustrating the microstructures of $SrTiO_3$ after 10 h at (a) 1350°C, (b) 1400°C and (c) 1425°C [10].

Figure 3. Example of a grain boundary groove measurement in $SrTiO_3$. Three profiles are extracted from the topographic AFM image in (a). The depth (d) and width (W) of the groove are measured from the topographic data. The results from the three profiles are averaged to determine the result for this grain boundary.

Figure 4. Grain orientation map of a single layer of the $SrTiO_3$ sample annealed at 1390 °C. Regions of the same orientation have the same color and the line segments approximating the grain boundaries are represented as black lines. Grains not touching an edge were labeled 'S' if they have an equivalent circular diameter < 5 μm and 'F' if they are larger. Four exemplary triple lines of different types are marked (see detailed explanation in text).

Figure 5. Grain sizes versus grain size rank for all of the grains within three parallel layers of the three-dimensional data. Grains touching the edge of the micrograph were ignored. There is an abrupt change in the slope at a diameter of about 5 μm, which we select as a condition to separate small and large grains.

Figure 6. Triple junction schematics. (a) Schematic defining energies and dihedral angles from Equation 3. (b) The ideal case for when three GB_{SS} meet. The ideal case for three GB_{FF} is analogous. (c) The ideal case for when a GB_{SS} (with lower relative energy) meets two

GB_{SF} boundaries. (d) The ideal case for when a GB_{FF}(with higher relative energy) meets two GB_{SF}.

Figure 7. Representative topographic AFM images of the samples annealed at (a) 1350 °C, (b) 1390 °C, and (c) 1400 °C.

Figure 8. Relative grain boundary energy distributions for the samples heated at 1350 °C, 1390 °C, and 1400 °C. Each point corresponds to a measured grain boundary groove and the points are ordered by relative energy.

Figure 9. Three-dimensional reconstruction of the microstructure of the $SrTiO_3$ sample annealed at 1390 °C. The grains are colored by orientation. The triple junction dihedral angles were calculated from these data.

Figure 10. Distribution of grain boundary dihedral angles for type SFF triple junctions, type SSF triple junctions, and the combined type SSS and FFF junctions.

Figure 11. Schematic diagram to explain the change in grain boundary energy within the anti-thermal region. The lines indicate the mean energies and the shaded bands indicate the range of energies resulting from anisotropic grain boundary energies. The lines are dashed when the complexion (based on its mean energy) is metastable and solid when it is stable.

References Cited

[1] J.E. Burke, D. Turnbull. Recrystallization and Grain Growth, Prog. Metal Phys. 3 (1952) 220-292, http://dx.doi.org/10.1016/0502-8205(52)90009-9.
[2] P.A. Beck, M.L. Holzworth, H. Hu. Instantaneous rates of grain growth, Phys. Rev. 73 (1948) 526-527, http://dx.doi.org/10.1103/PhysRev.73.526.
[3] P.A. Beck, J.C. Kremer, L. Demer. Grain growth in high purity aluminum, Phys. Rev. 71 (1947) 555-555, http://dx.doi.org/10.1103/PhysRev.71.555.
[4] R.C. Sun, C.L. Bauer. Tilt boundary migration in NaCl bicrystals, Acta Metall. 18 (1970) 639-647, http://dx.doi.org/10.1016/0001-6160(70)90093-3.

[5] R. Viswanathan, C.L. Bauer. Kinetics of grain-boundary migration in copper bicrystals with 001 rotation axes, Acta Metall. 21 (1973) 1099-1109, http://dx.doi.org/10.1016/0001-6160(73)90026-6.
[6] P.R. Cantwell, E.A. Holm, M.P. Harmer, M.J. Hoffmann. Anti-thermal behavior of materials, Scripta Mater. 103 (2015) 1-5, http://dx.doi.org/10.1016/j.scriptamat.2015.02.011.
[7] E.R. Homer, E.A. Holm, S.M. Foiles, D.L. Olmsted. Trends in Grain Boundary Mobility: Survey of Motion Mechanisms, JOM 66 (2014) 114-120, http://dx.doi.org/10.1007/s11837-013-0801-2.
[8] W. Rheinheimer, M.J. Hoffmann. Grain growth in perovskites: What is the impact of boundary transitions?, Curr. Opin. Solid State Mater. Sci. 20 (2016) 286-298, http://dx.doi.org/10.1016/j.cossms.2016.04.004.
[9] W. Rheinheimer, M.J. Hoffmann. Non-Arrhenius behavior of grain growth in strontium titanate: New evidence for a structural transition of grain boundaries, Scripta Mater. 101 (2015) 68-71, http://dx.doi.org/10.1016/j.scriptamat.2015.01.021.
[10] W. Rheinheimer, M.J. Hoffmann. Grain growth transitions of perovskite ceramics and their relationship to abnormal grain growth and bimodal microstructures, J. Mater. Sci. 51 (2016) 1756-1765, http://dx.doi.org/10.1007/s10853-015-9535-6.
[11] S.J. Dillon, M. Tang, W.C. Carter, M.P. Harmer. Complexion: A new concept for kinetic engineering in materials science, Acta Mater. 55 (2007) 6208-6218, http://dx.doi.org/10.1016/j.actamat.2007.07.029.
[12] P.R. Cantwell, M. Tang, S.J. Dillon, J. Luo, G.S. Rohrer, M.P. Harmer. Grain boundary complexions, Acta Mater. 62 (2014) 1-48, http://dx.doi.org/10.1016/j.actamat.2013.07.037.
[13] S.J. Dillon, M.P. Harmer, G.S. Rohrer. The Relative Energies of Normally and Abnormally Growing Grain Boundaries in Alumina Displaying Different Complexions, Journal of the American Ceramic Society 93 (2010) 1796-1802, http://dx.doi.org/10.1111/j.1551-2916.2010.03642.x.
[14] S.J. Dillon, M.P. Harmer, G.S. Rohrer. Influence of interface energies on solute partitioning mechanisms in doped aluminas, Acta Materialia 58 (2010) 5097-5108, http://dx.doi.org/10.1016/j.actamat.2010.05.045.
[15] S.A. Bojarski, M.P. Harmer, G.S. Rohrer. Influence of grain boundary energy on the nucleation of complexion transitions, Scripta Mater. 88 (2014) 1-4, http://dx.doi.org/10.1016/j.scriptamat.2014.06.016.
[16] S.A. Bojarski, S. Ma, W. Lenthe, M.P. Harmer, G.S. Rohrer. Changes in the Grain Boundary Character and Energy Distributions Resulting from a Complexion Transition in Ca-Doped Yttria, Metall. Mater. Trans. A 43A (2012) 3532-3538, http://dx.doi.org/10.1007/s11661-012-1172-y.
[17] O. Schumacher, C.J. Marvel, M.N. Kelly, P.R. Cantwell, R.P. Vinci, J.M. Rickman, G.S. Rohrer, M.P. Harmer. Complexion time-temperature-transformation (TTT) diagrams: Opportunities and challenges, Curr. Opin. Solid State Mater. Sci. 20 (2016) 316-323, http://dx.doi.org/10.1016/j.cossms.2016.05.004.
[18] S.-J. Shih, S. Lozano-Perez, D.J.H. Cockayne. Investigation of grain boundaries for abnormal grain growth in polycrystalline $SrTiO_3$, J. Mater. Res. 25 (2010) 260-265, http://dx.doi.org/10.1557/jmr.2010.0046.

[19] H. Sternlicht, W. Rheinheimer, M.J. Hoffmann, W.D. Kaplan. The mechanism of grain boundary motion in $SrTiO_3$, J. Mater. Sci. 51 (2016) 467-475, http://dx.doi.org/10.1007/s10853-015-9058-1.

[20] D. Gupta. Diffusion, solute segregations and interfacial energies in some material: An overview, Interface Sci. 11 (2003) 7-20, http://dx.doi.org/10.1023/a:1021570503733.

[21] M.N. Kelly, S.A. Bojarski, G.S. Rohrer. The temperature dependence of the relative grain-boundary energy of yttria-doped alumina, J. Am. Ceram. Soc. 100 (2017) 783-791, http://dx.doi.org/10.1111/jace.14488.

[22] G.S. Rohrer. The role of grain boundary energy in grain boundary complexion transitions, Curr. Opin. Solid State Mater. Sci. 20 (2016) 231-239, http://dx.doi.org/10.1016/j.cossms.2016.03.001.

[23] D.M. Saylor, G.S. Rohrer. Measuring the influence of grain-boundary misorientation on thermal groove geometry in ceramic polycrystals, J. Am. Ceram. Soc. 82 (1999) 1529-1536, http://dx.doi.org/.

[24] D. Necas, P. Klapetek. Gwyddion: an open-source software for SPM data analysis, Cent. Eur. J. Phys. 10 (2012) 181-188, http://dx.doi.org/10.2478/s11534-011-0096-2.

[25] W.W. Mullins. Theory of thermal grooving, J. Appl. Phys. 28 (1957) 333-339.

[26] S.J. Dillon, G.S. Rohrer. Characterization of the Grain-Boundary Character and Energy Distributions of Yttria Using Automated Serial Sectioning and EBSD in the FIB, J. Am. Ceram. Soc. 92 (2009) 1580-1585, http://dx.doi.org/10.1111/j.1551-2916.2009.03064.x.

[27] J. Li, S.J. Dillon, G.S. Rohrer. Relative grain boundary area and energy distributions in nickel, Acta Mater. 57 (2009) 4304-4311, http://dx.doi.org/10.1016/j.actamat.2009.06.004.

[28] M.N. Kelly, K. Glowinski, N.T. Nuhfer, G.S. Rohrer. The five parameter grain boundary character distribution of alpha-Ti determined from three-dimensional orientation data, Acta Mater. 111 (2016) 22-30, http://dx.doi.org/10.1016/j.actamat.2016.03.029.

[29] C.S. Smith. Grains, phases, and interfaces - an interpretation of microstructure, T. Am. I. Min. Met. Eng. 175 (1948) 15-51, http://dx.doi.org/.

[30] S.J. Dillon, M.P. Harmer, G.S. Rohrer. The Relative Energies of Normally and Abnormally Growing Grain Boundaries in Alumina Displaying Different Complexions, J. Am. Ceram. Soc. 93 (2010) 1796-1802, http://dx.doi.org/10.1111/j.1551-2916.2010.03642.x.

[31] S.M. Foiles. Temperature dependence of grain boundary free energy and elastic constants, Scripta Mater. 62 (2010) 231-234, http://dx.doi.org/10.1016/j.scriptamat.2009.11.003.

[32] R. Najafabadi, H.Y. Wang, D.J. Srolovitz, R. Lesar. The effects of segregation on grain-boundary cohesive energies in $Ni_{3-1}Al_{1+x}$, Scripta Metall. Mater. 25 (1991) 2497-2502, http://dx.doi.org/10.1016/0956-716x(91)90056-7.

[33] S.M. Foiles. Evaluation of harmonic methods for calculating the free-energy of defects in solids, Phys. Rev. B 49 (1994) 14930-14938, http://dx.doi.org/10.1103/PhysRevB.49.14930.

[34] S.J. Dillon, M.P. Harmer. Demystifying the role of sintering additives with "complexion", J. Eur. Ceram. Soc. 28 (2008) 1485-1493, http://dx.doi.org/10.1016/j.jeurceramsoc.2007.12.018.

[35] M. Tang, W.C. Carter, R.M. Cannon. Grain boundary transitions in binary alloys, Phys. Rev. Lett. 97 (2006) 4, http://dx.doi.org/075502
10.1103/PhysRevLett.97.075502.

[36] T. Sano, D.M. Saylor, G.S. Rohrer. Surface energy anisotropy of SrTiO3 at 1400 degrees C in air, Journal of the American Ceramic Society 86 (2003) 1933-1939, http://dx.doi.org/.

[37] D.M. Saylor, B. El Dasher, T. Sano, G.S. Rohrer. Distribution of grain boundaries in $SrTiO_3$ as a function of five macroscopic parameters, J. Am. Ceram. Soc. 87 (2004) 670-676, http://dx.doi.org/.

[38] W. Rheinheimer, M. Baeurer, H. Chien, G.S. Rohrer, C.A. Handwerker, J.E. Blendell, M.J. Hoffmann. The equilibrium crystal shape of strontium titanate and its relationship to the grain boundary plane distribution, Acta Materialia 82 (2015) 32-40, http://dx.doi.org/10.1016/j.actamat.2014.08.065.

[39] G.S. Rohrer. Grain boundary energy anisotropy: a review, J. Mater. Sci. 46 (2011) 5881-5895, http://dx.doi.org/10.1007/s10853-011-5677-3.

[40] D.M. Saylor, A. Morawiec, G.S. Rohrer. Distribution and energies of grain boundaries in magnesia as a function of five degrees of freedom, J. Am. Ceram. Soc. 85 (2002) 3081-3083, http://dx.doi.org/.

[41] S.J. Dillon, G.S. Rohrer. Mechanism for the development of anisotropic grain boundary character distributions during normal grain growth, Acta Mater. 57 (2009) 1-7, http://dx.doi.org/10.1016/j.actamat.2008.08.062.